Physiological Measurement

IPEM
Institute of Physics and Engineering in Medicine

Dependent component analysis for the magnetogastrographic detection of human electrical response activity

IOP PUBLISHING PHYSIOLOGICAL MEASUREMENT

Physiol. Meas. **28** (2007) 1029–1044 doi:10.1088/0967-3334/28/9/005

Dependent component analysis for the magnetogastrographic detection of human electrical response activity

C A Estombelo-Montesco[1], D B de Araujo[1], A C R Silva Filho[1], E R Moraes[1], A K Barros[2], R T Wakai[3] and O Baffa[1]

[1] Department of Physics and Mathematics, FFCLRP, University of São Paulo, 14040-901 Ribeirão Preto, SP, Brazil
[2] Department of Electrical Engineering, Federal University of Maranhão, 65075-460 Sao Luis, Maranhão, Brazil
[3] Department of Medical Physics, Medical School, University of Wisconsin, Madison, WI 53706-2413, USA

E-mail: baffa@usp.br

Received 29 March 2007, accepted for publication 27 June 2007
Published 21 August 2007
Online at stacks.iop.org/PM/28/1029

Abstract

The detection of the basic electric rhythm (BER), composed of a 3 cycles min^{-1} oscillation, can be performed using SQUID magnetometers. However, the electric response activity (ERA), which is generated when the stomach is performing a mechanical activity, was detected mainly by invasive electrical measurements and only recently was one report published describing its detection by magnetic measurements. This study was performed with the aim of detecting the ERA noninvasively after a meal. MGG recordings were made with a 74-channel first-order gradiometer (Magnes II, biomagnetic technologies) housed in a shielded room. Seven nonsymptomatic volunteers were measured in the study. Initially a 10 min recording was performed with the subject in the fasted state. A 250 kcal meal was given to the subject without moving out of the magnetometers and two epochs of 10 min each were acquired. The signals were processed to remove cardiac interference by an algorithm based on a variation of independent component analysis (ICA), then autoregressive and wavelet analysis was performed. Preliminary results have shown that there is an increase in the signal power at higher frequencies around (0.6 Hz–1.3 Hz) usually associated with the basic electric rhythm. The center of the frequency band and its width varied from subject to subject, demonstrating the importance of pre-prandial acquisition as a control. Another interesting finding was an increase in power after about 5 min of meal ingestion. This period roughly agrees with the lag phase of gastric emptying, measured by scintigraphy and other techniques. We confirm that MGG can detect the electric response activity in normal volunteers. Further improvements in signal

processing and standardization of signal acquisition are necessary to ascertain its possible use in clinical situations.

Keywords: magnetogastrography, gastric electrical response activity, spike activity, stomach, independent component analysis, autoregressive methods, Morlet wavelet

1. Introduction

The first non-invasive measurement of the stomach's electrical activity was made by Alvarez in 1922. Since then this field has grown considerably due to the extensive exploration of information from electrogastrography (EGG) and more recently from magnetogastrography (MGG) (Bradshaw *et al* 2006, Moraes *et al* 2003, Moraes and Baffa 1999).

EGG studies in the 1950s revealed that the stomach was electrically active and that the slow-wave depolarization of this activity is generated by a neural network called the interstitial cells of Cajal (ICC). This network resides between two muscle layers (the longitudinal and circular muscles) and at submucosal borders of the circular muscle. It is assumed that the electrical rhythm is propagated via electrical coupling between the neurons of this extensive ICC network and is thus carried throughout the gastrointestinal (GI) tract with different frequencies (Akin and Sun 1999).

Usually EGG signals are obtained with cutaneous electrodes positioned on the upper abdomen. While the literature shows many contributions leading to a better understanding of gastric electrical activity (GEA), the EGG is difficult to measure, mostly because it is superimposed with other electrical signals that are difficult to discriminate (Irimia *et al* 2006). Moreover Akin and Sun (1999) state that the real problem lies not in employing the proper analysis method but in data acquisition, suggesting that further work is needed to improve data acquisition.

The MGG records the magnetic field produced by the GEA, and has been measured using SQUID (superconducting quantum interference device) magnetometers. The magnetic signals are less affected by tissue conductivity than the electric signals and show a stronger dependence of the source-to-magnetometers distance (Andrä and Nowak 2006). MGG, thus, can provide higher spatial resolution than EGG (Andrä and Nowak 2006).

MGG already has clinical relevance. Some evidence suggests that functional gastrointestinal disorders are often related to gastric motility impairment (or mechanical activity) (Chen and McCallum 1993). Hence, detection of motility disorders, even via such indirect means as MGG, has an important diagnostic value.

Previous invasive studies have shown that the electrical extracellular signal detected with serosal electrodes has two distinct components. One, often referred to as 'electrical control activity' (ECA), is an omnipresent periodic activity not necessarily related to contractile motion. ECA has also been called the 'basic electrical rhythm' (BER), 'slow wave depolarization', or simply 'slow wave'. The second component, called electrical response activity (ERA), is time locked to the ECA, but only occurs in conjunction with phasic contractile activity (Smout *et al* 1980). ERA has also been named 'spike-like action potentials' (SLAP) or just 'spike activity' (Akin and Sun 1999). To summarize, the phenomenon of gastric electrical activity consists of two important components to be explored in this work: an ECA that manifests itself as an electric slow wave (with a frequency of three cycles per minute in humans) and an ERA which, according to the literature and invasive methods, is characterized

by spiking potentials during the plateau phase of the ECA (Irimia *et al* 2006). A better characterization of this ERA is considered a subject of major importance that had not been investigated satisfactorily in noninvasive human studies.

In addition, it has been observed invasively that contractions are the product of high frequency action potentials either superimposed on the plateau phases, or occurring between slow-wave depolarizations (Liu *et al* 1995). Interestingly, if spike activity has both a high power intensity and a long duration then the contractions are stronger (Akin and Sun 1999).

Unfortunately, MGG signals are highly contaminated by respiration, motion and cardiac artifact and possibly by myoelectrical activity from other organs, which confound MGG interpretation and analysis (Liang *et al* 2000). Detection of ERA is especially difficult because its low amplitude and spectral overlap with cardiac signals precludes the use of most standard analysis methods (Akin and Sun 1999).

Recently, major advances in signal processing have been achieved with blind source separation (BSS), which has been successfully used to separate signal from interference in a number of paradigms, including biomedical signal processing. BSS is based on the assumption that the detected signals are a mixture of a small number of independent source signals that are linearly combined via an unknown mixing matrix. BSS seeks to determine the mixing matrix and to recover the source signals based on principles of statistical independence. In most cases, extraction of all the source signals is unnecessary; instead, *a priori* information can be applied to extract only the signal of interest.

Here we propose a strategy based on the algorithm of Barros and Cichocki (2001), and de Araujo *et al* (2005) to separate the ECA and ERA signal from the other interferences, even in cases of low signal-to-noise ratio, which we call dependent component analysis (DCA). For a quasi-periodic signal, DCA identifies the signal component based on the time delay determined from the temporal characteristics of the ECA in the MGG measurement. The delay is determined by finding the poles of the autocorrelation function after modeling the signal using autoregressive analysis. Furthermore, we used a time–frequency representation of such signal, based on wavelet transforms, to examine temporal characteristics of ERA.

2. Material and methods

2.1. MGG signal acquisition

The recordings were made with a 74-channel first-order gradiometer system (Magnes, Biomagnetic Technologies, Inc) housed within a magnetic shielded room. The system consists of two magnetometer units, A and B, each containing 37 channels uniformly distributed over circular areas of diameters 13.7 and 14.4 cm, respectively. A is a floor-standing unit and B is attached to a ceiling-mounted gantry. The intrinsic noise per channel is 5–10 fT $Hz^{-1/2}$.

Seven asymptomatic subjects volunteered for the study. The gradiometer was positioned as shown in figure 1. A horizontal line was drawn at half the distance from the umbilicus to the xiphoid process, and the gradiometer array was centered at half the distance to the first rib.

The subjects lay with their stomach over the B magnetometer through a special bed with an opening such that the stomach could lie directly on the B magnetometer. The A magnetometer was positioned over the back of the subject. With this experimental arrangement it was possible to simultaneously acquire signals in the front and back of the stomach; moreover, it was possible to acquire signals from the stomach at the closest possible distance.

Three epochs of 10 min duration were acquired. The first was acquired before the ingestion of the test meal (pre-prandial). After that, a standard test meal comprised of a cheese sandwich

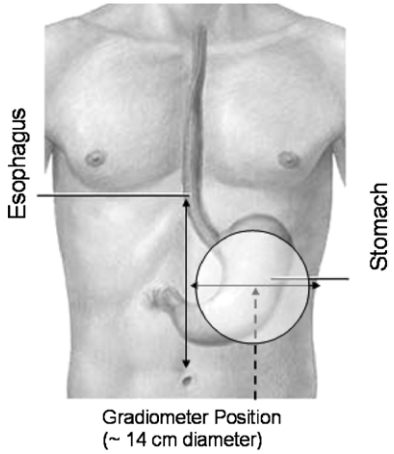

Figure 1. Positioning of magnetometer unit A. Unit B was positioned on the back of the subject aligned with unit A.

of 250 kcal (110 kcal bread + 140 kcal cheese) was given to the subjects immediately before the second measurement (first post-prandial). Then, a second 10 min acquisition was made (second post-prandial).

The dc-coupled MGG signals were sampled at 73.1 Hz and stored for subsequent analyses. The digitized data were decimated to 4 Hz to eliminate higher frequency artifacts and interference; this resulted in a signal bandwidth of just less than 1 cycle min $^{-1}$.

2.2. Blind source separation using temporal structure

One of the most common models of blind source separation (BSS) assumes that the signal is linear mixture of independent random sources. While BSS can be applied regardless of the temporal structure of the signal, the presence of temporal structure can aid in isolating the component of interest. For example, the autocorrelation (correlation over different time lags) can be used to create a filter to extract a source component having a characteristic time delay. Then we can use additional statistics to improve the estimation of the source component from the model in cases where basic methods cannot estimate it. For instance, if the components are Gaussian but correlated over time, then other physiological components without this temporal structure can be removed.

The proposed strategy to extract ECA and ERA components is based on the dependent component analysis (DCA) method. DCA is a method based on multivariate analysis that uses *a priori* the delay based on the temporal characteristics of the ECA and ERA signal to be extracted (see figure 2). The method for extraction and artifact removal is fully described in de Araujo *et al* (2005) and a short description follows. Consider n sources $\mathbf{S} = [s_1, s_2, \ldots, s_n]^T$ that are mixed into vector x through the following linear combination:

$$\mathbf{X} = \mathbf{AS}, \tag{1}$$

where $\mathbf{A}$ is an $n \times n$ invertible matrix. Our goal here is to find the source of interest, s_i. In general, the number of independent components can be as large as the dimension of $\mathbf{X}$.

The method proposed by Barros and Cichocki (2001) aims at extracting only the desired component with a given characteristic, instead of all sources, and has been successfully applied to other applications (de Araujo *et al* 2005). The method can be described briefly as follows.

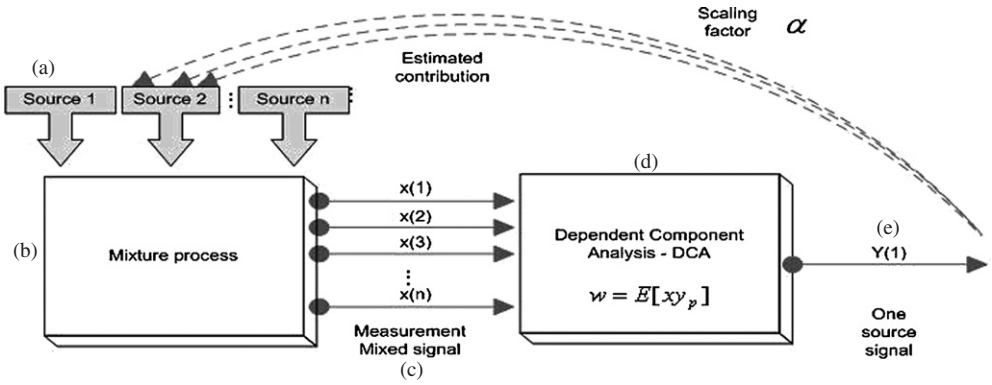

Figure 2. Schematics for scaling factor determination. (a) First each source (stomach, heart, tissue, artifacts, etc) produces a magnetic signal, actually not seen directly. (b) Then each source is mixed with other sources, in our case we consider a linear mixture and it is represented by the block mixture process. (c) When the signals are acquired actually we are measuring the signals from the mixture process obtaining one time series for each magnetometer. (d) Then separation/extraction of the source of interest can be done and further evaluated through DCA process using equation (2). (e) At the output there is a single time series of interest where a scale factor needs to be calculated to estimate the relative amplitude. These steps were applied for every epoch: pre- and post-prandial measurements.

As we wish to extract only a single source, we can write the signal as $y(k) = w^T x(k)$, where w is a weight vector for that single source. Defining the error as $\varepsilon_a(k) = y(k) - y(k-p)$ and minimizing the mean squared error $\xi(w) = E\left[\varepsilon_a^2\right]$, we find

$$w = E[xy_p], \tag{2}$$

where $y_p = y(k-p)$. We use sequential signal extraction along with *a priori* information about the autocorrelation function. One practical problem is how to estimate the optimal time delay. A simple solution is to calculate the autocorrelation function of the magnetometer signals and find the feature, in our case a peak with appropriate time lag, corresponding to the signal of interest. In order to accomplish this, we model the system using autoregression, as described in the next section.

2.3. The adaptive autoregressive model for spectrum estimation

Given a time series, an autoregressive (AR) model predicts the next observation based on a weighted sum of the preceding data. Thus, the AR coefficients (weights) characterize the time series. Furthermore, previous works (Moraes *et al* 2003) suggest that the AR spectrum estimator provides more detailed qualitative information about frequency variations of short duration signals than the FFT method for analysis of human MGG data.

Power spectra have a well-defined physical meaning (Kato *et al* 1996) and often we can infer the behavior of the system from the analysis (de Araujo *et al* 2005, Moraes *et al* 2003). The power spectrum density (PSD) of the process modeled by an AR(p) model is given by Moraes *et al* (2003), Madisetti and Williams (1999):

$$P_m(\omega) = \sigma^2 \left| 1 + \sum_{k=1}^{p} a_{mk} \exp(-\mathrm{i}\omega k) \right|^{-2} \tag{3}$$

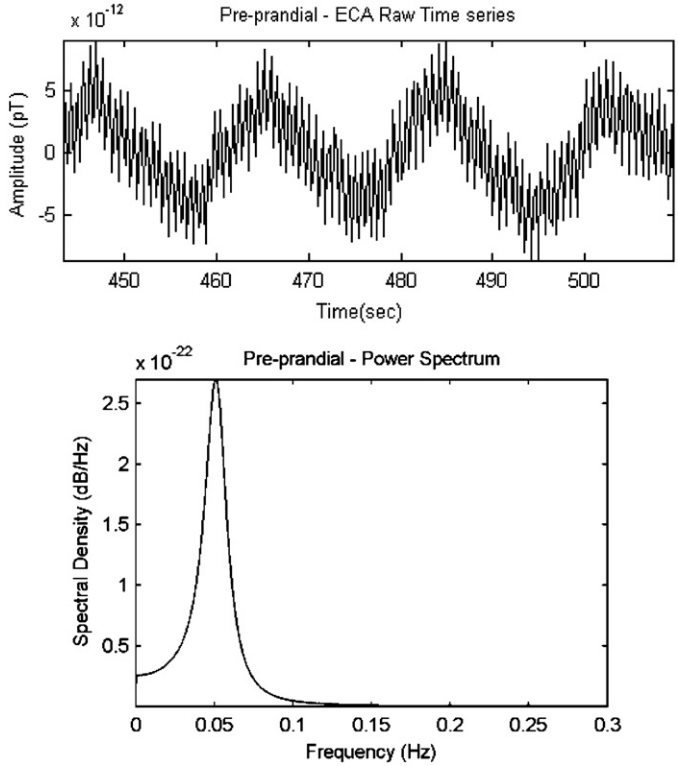

Figure 3. The upper panel shows the ECA raw time series after decimation. The lower panel shows the ECA power spectrum of a pre-prandial single recording from raw data. The ECA signal is present at 0.05 Hz (3 cpm).

where $P_m(\omega)$ is the PSD at the angular frequency ω of the point $x(m)$, a_{mk} are the AR coefficients of AR(p) and σ^2 is the variance of noise. The power spectrum described here will be used to estimate the optimal time delay (before DCA filtering) for each desired component and to compare energies of the estimated source signals in pre-prandial versus post-prandial measurements.

In figures 3 and 4 we show representative power spectra of segments of the raw signal from a pre-prandial recording. From the model we can estimate an appropriate time delay of the signal of interest to be extracted. Figure 3 shows the power spectrum of the ECA signal present at 0.05 Hz (or 3 cpm). This *a priori* information is used to estimate the time delay for DCA filtering.

The ERA and heart power spectrum of a pre-prandial single recording is shown in figure 4. It can be seen that the heart component is much (1.5 Hz) stronger than the ERA (0.8 Hz) activity.

In contrast, the power spectra of post-prandial recordings are shown in figures 5 and 6. These representative power spectra show peaks near 0.8 Hz, indicating a different state compared to pre-prandial measurement in figure 4. Furthermore, the power associated with ERA activity in the post-prandial stage is higher than in the pre-prandial stage at the same frequency.

Since the autoregressive model uses a segment of raw signal we cannot be certain of the existence of ERA at all. MGG signals are contaminated by cardiac signals, i.e. the

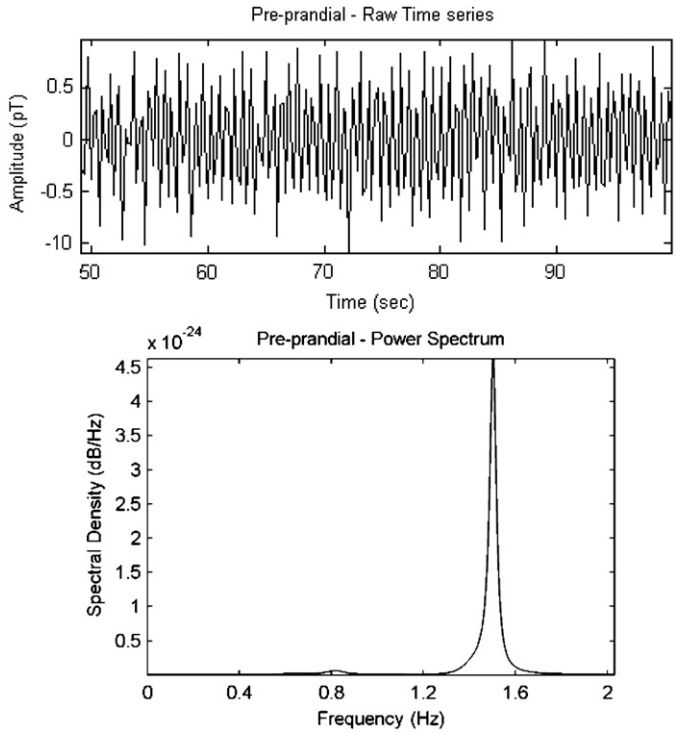

Figure 4. The upper panel shows pre-prandial raw time series after decimation and low frequency filtered. The lower panel shows the ERA power spectrum of the pre-prandial recording from raw data shown in the upper panel. The ERA signal has weak energy compared to the heart component at higher frequency.

magnetocardiogram (MCG), that extend over a wide frequency range (Irimia *et al* 2006), overlapping with the ERA frequency range. Another issue noted in the literature is that the power of the ERA signal can fluctuate.

2.4. Avoiding scaling factor problem by projection approach

The estimation of the signal extracted by DCA might be scaled at the output. Subsequently this estimation can lead to an erroneous comparison between pre-prandial and post-prandial energies if we do not determine the proper scale factor. To overcome this problem we need an estimation method for the scale factor for each signal component extracted by DCA.

Consider from equation (2) an output vector, $y = wx = wAs$. It has an indeterminacy that can be expressed as $y = \alpha s$, where α is a scaling factor that needs to be estimated for the signal extracted from each epoch (see figure 2).

After extracting the desired source component, y, one can project the source signal of interest back onto magnetometer array signals, calculating the scale factor as follows. First let us define the following error:

$$\varepsilon_b = x_i - \alpha_i y, \tag{4}$$

where x_i is the desired signal and y is the output of the DCA filter. Next, we estimate a scale factor α_i that minimizes the mean squared error $\xi(\alpha_i) = E\left[\varepsilon_b^2\right]$, and we obtain $\xi(\alpha_i) = x_i^2 - 2x_i\alpha_i y + (\alpha_i y)^2$. The minimum will be reached yielding the following scale factor:

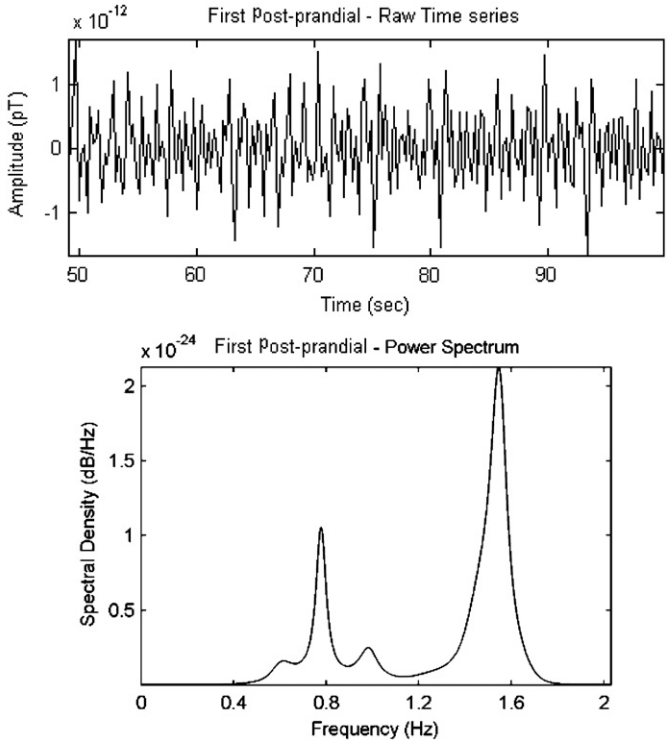

Figure 5. The upper panel shows the first post-prandial raw time series after decimation and low frequency filtering. The lower panel shows the ERA power spectrum of a first post-prandial recording from raw data. The ERA is present; peaks corresponding to the ERA and heart components are seen.

$$\alpha_i = E[y^2]^{-1} E[xy]. \tag{5}$$

The scaling factor provides two valuable pieces of information. First, if we take the high absolute value of α, then we have the scaling factor for the output of DCA (estimated source signal). Therefore, we can compare their relative amplitudes in the time or frequency domain, and detect the ERA signal. Second, we can get the contribution from each channel to the source signal. This allows spatial mapping over 37 channels of the estimated source signal.

2.5. Time–frequency representation of spike activity

Another method used to quantify changes in spike activity is time–frequency representation (TFR), such as wavelet decomposition. This method provides a better compromise between time and frequency resolution than other methods such as short-term Fourier transforms. It provides the time-varying energy of the signal in each frequency band, leading to a TF representation signal (Jensen *et al* 2002, TallonBaudry *et al* 1997).

Wavelets are functions that decompose the data into frequency components in a manner similar to Fourier analysis. As sine and cosine functions are periodic out to infinity, they are a poor approximation for sharp spikes. With wavelets it is possible to use functions that are confined to finite domains. This enables them to perform well on discontinuities and sharp spikes.

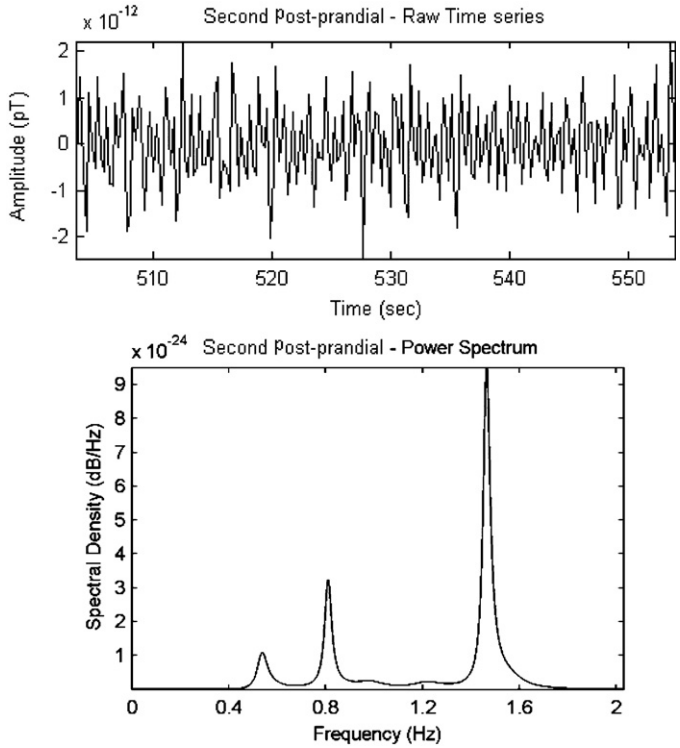

Figure 6. The upper panel shows the second post-prandial raw time series after decimation and low frequency filtering. The lower panel shows the ERA power spectrum of a second post-prandial recording from raw data. Again, the ERA is present, as well as heart components.

Many wavelet bases have been devised. In this study, the wavelet utilized in calculating TFRs is a Morlet wavelet, calculated according to the formula (Jensen *et al* 2002, TallonBaudry *et al* 1997)

$$\varphi(f_0, t) = A_\varphi \cdot \mathrm{e}^{\frac{-t^2}{2\sigma_t^2}} \cdot \mathrm{e}^{\mathrm{i}2\pi f_0 t}, \tag{6}$$

where $\sigma_t = \frac{1}{2\pi\sigma_f}$ is the time of the wavelet and σ_f is the frequency of the wavelet. Wavelets are normalized so that their total energy is 1, the normalization factor A being equal to

$$(\sigma_t\sqrt{\pi})^{-1/2}. \tag{7}$$

A wavelet family is characterized by a constant ratio (f_0/σ_f) (dimension ratio defined to be ω), which in practice should be chosen to be greater than $\sim$5 (TallonBaudry *et al* 1997), where ω is called the 'width' of the wavelet and f_0 is the frequency for which the wavelet transformation is performed (Toni 2002). The time resolution of this method thus increases with frequency, whereas the frequency resolution decreases.

3. Results

3.1. ECA and ERA Components by DCA

Figure 7 shows the ECA and ERA components extracted at each epoch by DCA. Generally, the ECA component has higher amplitude than the ERA component. However, for visual

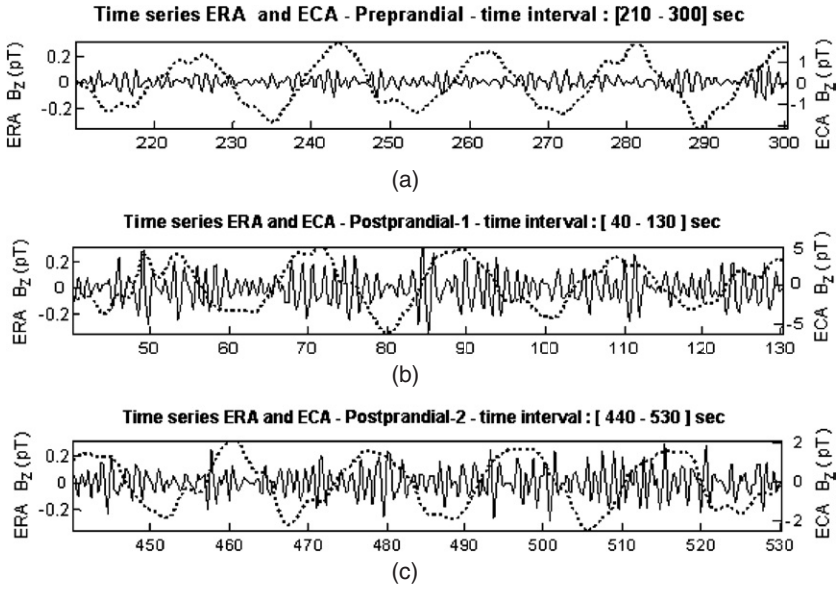

Figure 7. ECA (dotted line) and ERA (solid line) signals extracted using DCA processing. (a) Extracted components for the pre-prandial epoch, (b) and (c) show extracted components for the first and second post-prandial epochs. The right side shows the ECA scale and left side shows the ERA scale. The ECA signal component consists of an upstroke followed by a plateau and then by a slow depolarization phase with an approximate frequency of 3 cpm. Note the difference of amplitude between the ERA signals in pre-prandial epoch and the ERA signals of the two post-prandial epochs. The *x*-scale is in seconds.

purposes it is better to superimpose one component on top of the other, each one with their own scale. Figure 7 shows the extracted components for the pre-prandial epoch (a) and the extracted components for the first and second post-prandial epochs (b and c). Figure 7 shows the ECA component (dotted line) and the ERA component (solid line).

Figures 7(b) and (c) show that ECA components are always present in the stomach. Furthermore, it can be noted that post-prandial ERA components have higher amplitude than the pre-prandial components (figure 7(a)), especially during the plateau phase of the ECA near 50 s, 70 s, 90 s and 110 s of figure 7(b).

The energy contribution from each channel can be used to construct isocontribution maps. These contributions show a spatial representation of the area where the source signal came from. The representation of the 37 channel layout from ECA (pre-prandial and post-prandial epoch) is shown in figure 8.

Figure 9(a) shows the contribution of each channel after DCA processing to extract the ERA signal in the pre-prandial epoch. One observes a low energy for the ERA process. The small amount of energy at the top right corner is from cardiac signal.

Figure 9(b) shows the post-prandial epoch and the localization of ERA after DCA extraction. An increase in the contribution energy in a number of channels on right side is observed, whereas the contribution of these channels was low in the pre-prandial epoch.

The upper diagram of figure 10 shows the ERA and ECA components during a pre-prandial epoch. The lower diagram of figure 10 shows a white solid line, obtained by summing the ERA and ECA time series, superimposed on the time–frequency representation of the ERA component, obtained by the wavelet transformation. The *y*-scale of the TFR is from 0.5 Hz

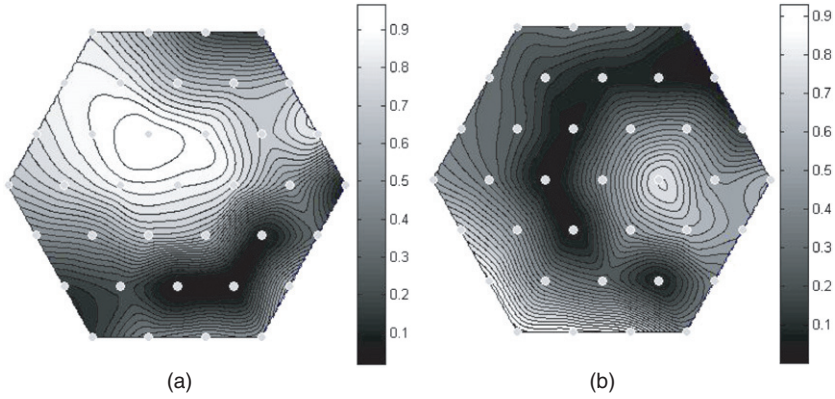

Figure 8. Channel contribution of the extracted ECA component. (a) The isocontribution map of ECA signal from the pre-prandial epoch. (b) The isocontribution map of the ECA signal from a post-prandial epoch. In these epochs the intense energy of the slow wave is present at all times.

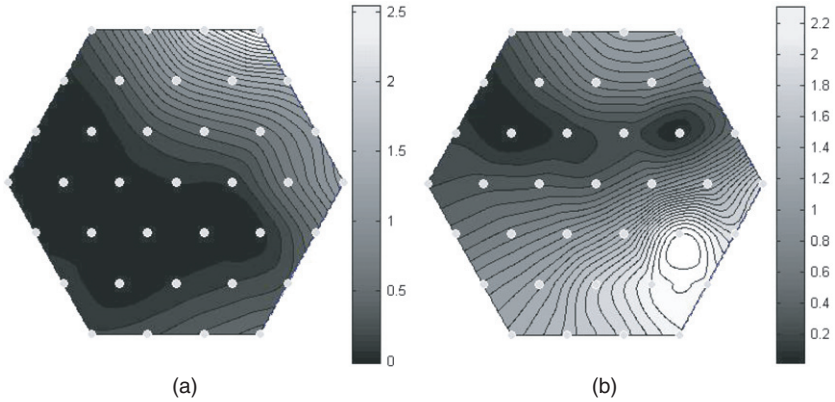

Figure 9. Channel contribution of the extracted ERA component. (a) The isocontribution map of the ERA signal from the pre-prandial epoch. The ERA is expected to show no contribution because there is no contraction during the pre-prandial epoch. (b) The contribution map of ERA signal from the first post-prandial epoch.

to 1.3 Hz. A few localized high energy regions can be observed for the ERA component, but they are not consistently time locked with the ECA component.

Figure 11, upper panel, shows the ERA and ECA components during the first post-prandial epoch. The amplitude of the ERA component is greater here than during the pre-prandial epoch. The lower panel of figure 11 shows high energy spots of the ERA component that are time locked with the ECA component. This characteristic is very important to verify the existence of the ERA component. Another characteristic to note is the fundamental frequency of the ERA component; although it concentrates at 0.8 Hz it can vary with time, increasing up to 1.30 Hz, but it preserves the time-locking with the ECA component at the plateau.

Figure 12, upper diagram, shows the ERA and ECA components during the second post-prandial epoch. We can observe that the ERA amplitude remains high, as in the first post-prandial epoch. Differences can be easily seen in the lower diagram of figure 12, as

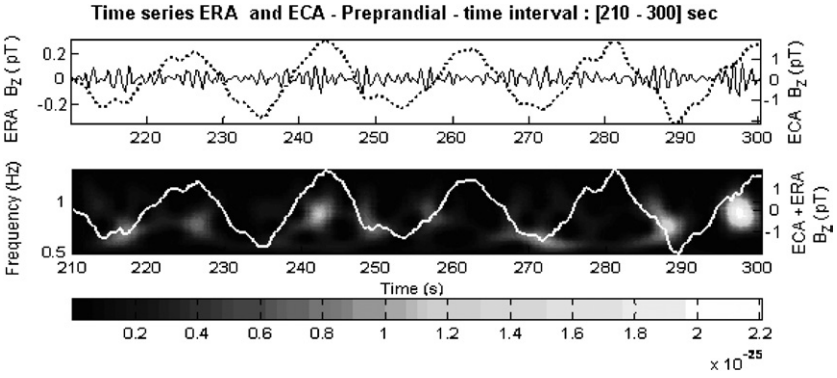

Figure 10. A time interval during the pre-prandial epoch with the ECA and ERA components in the upper panel and the TFR of the ERA component in the lower panel. Superimposed on the TFR with a solid line is the sum of the ECA component plus the ERA component, which are shown in the upper panel. The scale of the left side is for the TFR of the ERA and the scale on the right side is for the summed time series.

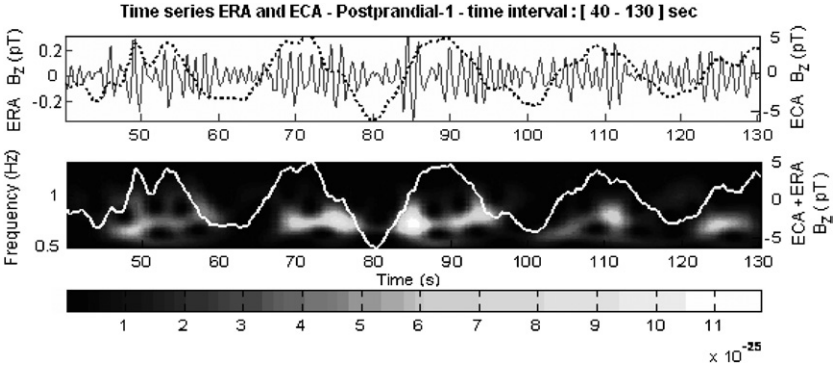

Figure 11. A time interval during the first post-prandial epoch with ECA and ERA components. In the upper panel the spikes of the ERA component can be observed, which are reflected in the TFR in the lower panel and are time locked with the ECA component. The frequency of the ERA component in the TFR varies from 0.6 Hz to 1.0 Hz. The scales of this figure are similar to those of figure 10.

the TFR of the ERA component has a more diffuse energy distribution than in the previous epoch. However, it still preserves the time locking with the ECA component, despite the energy decrease.

After extracting the desired source with DCA and estimating the scale factor, we can calculate the adaptive power spectrum to determine the energy for each epoch using the autoregressive (AR) method. The results show an amplitude increase of the signal around (0.6 Hz–1.0 Hz) (figure 13) with a dominant frequency at 0.8 Hz, usually correlated with the higher intensity of the ECA rhythm. The center of the frequency band and its width varied from one subject to another, showing the importance of the pre-prandial acquisition as a control. Another interesting observation is an increase in power after about 5 min of meal ingestion. This period roughly agrees with the time lag of gastric emptying, measured by scintigraphy and other techniques, for a solid meal.

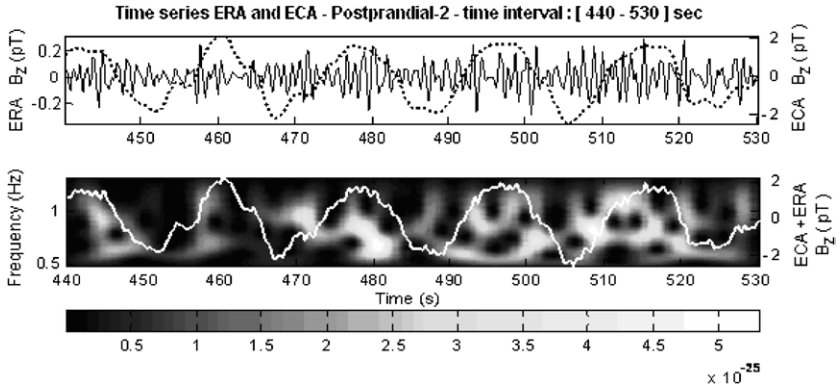

Figure 12. A time interval during the second post-prandial epoch with ECA and ERA components. Here the major difference is found for the ERA component; it is more distributed in both time and frequency but we can see that it is still time locked with the ECA component.

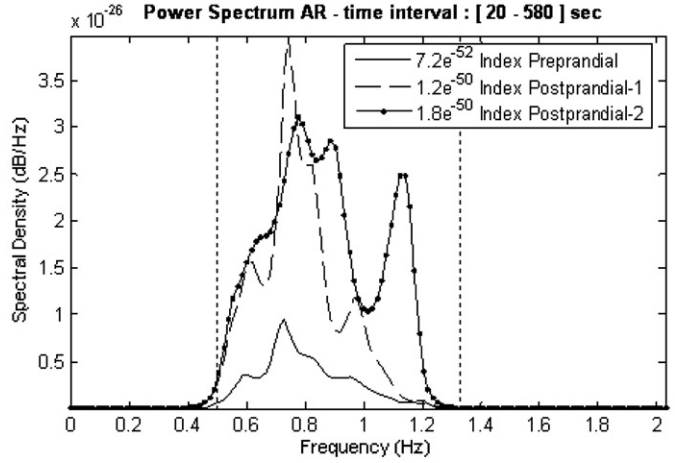

Figure 13. Autoregressive power spectrum of pre-prandial and post-prandial epochs after signal extraction from one subject. The inset shows the index of each epoch.

The integrated power spectrum in the frequency band of 0.5 Hz to 1.33 Hz was used to generate an index of ERA. Signal acquired from all volunteers shown an increment of ERA index, when the pre- and post-prandial were compared. These results can be seen in table 1.

4. Discussion

Some authors (Akin and Sun 1999) consider signal acquisition the main obstacle to obtaining reliable information about the stomach's electrical activity. Taking into account that MGG has a higher source-to-magnetometer distance sensitivity than EGG, that magnetic fields do not depend on the permeability of biological tissues, which is nearly equal to that of free space, it can be inferred that MGG is an excellent tool for signal acquisition with a good signal-to-noise ratio.

Table 1. Index for each epoch (between 0.5 Hz and 1.33 Hz) $\times 10^{51}$.

	Pre-prandial	Post-prandial (1)	Post-prandial (2)
Volunteer 1	8.0	1100	930
Volunteer 2	0.72	12	18
Volunteer 3	9.0	91	120
Volunteer 4	27	29	44
Volunteer 5	16	300	83
Volunteer 6	4.2	2800	5100
Volunteer 7	8.6	99	180

In the post-prandial epochs, which consisted of a longer time series, the center frequency of the ERA component fluctuated between 0.6 Hz and 1 Hz with a dominant frequency of 0.8 Hz. This variation can be observed in the time–frequency representation using Morlet wavelets, with its superior time and frequency localization properties, as shown in figures 11 and 12 compared with figure 10. Moreover, it can be observed that the energy in various frequency bands between pre-prandial and post-prandial is different, meaning that there is some energy frequency redistribution in the post-prandial stage. This information could have diagnostic value because such redistribution may be different in abnormal states.

The time locking of the ERA and ECA signal can also be observed in some epochs. This representation avoids the problem mentioned in Akin and Sun (1999), namely the shifting in the frequency locus of the spike activity caused by delay of the EGG measurement. To account for this delay one must consider how the tissue layers affect the propagation of serosal and surface signals, a problem not solved yet.

Figure 13 shows the difference in the power spectra of spikeless and spiked data corresponding to pre-prandial and post-prandial epochs, respectively, where the latter shows an increase of energy. Similar approach has been used in another work with no successful results (Akin and Sun 1999) for EGG signals; thus the MGG signals recorded here showed better signal-to-noise ratio and allowed the detection of the spike activity by applying the AR method.

In the present study, the amplitudes of the ECA and ERA signals were different, especially in comparison with the cardiac signal. If we consider the position of the magnetometer and the spatial dependences of the magnetic signals, it is confirmed that the ECA signal is stronger than other components, and sometimes it can be seen without any signal processing. But the ERA signal, in contrast with another report (Irimia *et al* 2006), is less intense than the ECA signals, and especially when compared with the cardiac signal. The cardiac signal spans a wide range of frequencies, masking the ERA signal. This substantiates the hypothesis made in Akin and Sun (1999) and by other investigators regarding the existence of an ERA signal with small amplitude and high frequency content that might be responsible for triggering the contractions. Moreover, due to the overlap of the cardiac and ERA signals in the frequency domain, it is not possible to use a classical filter to remove the cardiac component. Finally, analysis of MGG signals is complicated by biological interferences such as respiration, small and large intestine and duodenum magnetic signals.

These difficulties were overcome by using DCA to extract only the desired component with a specified periodicity, rather than extracting all sources. DCA can be applied even to a low signal-to-noise ratio recording. One problem, however, is that the scale of the extracted component can be altered, leading to an inaccurate energy. To avoid the scaling factor problem, a projection approach can be applied. Generally scaling factors have not been a problem in many applications of BSS that involve a single measurement or experimental condition.

But this is not the case in our study, which includes three epochs, one pre-prandial and two post-prandial. It is therefore necessary to compute the scaling factor to obtain coherent relative amplitudes for each epoch, which was accomplished here by the projection approach.

A previous work (Irimia *et al* 2006), utilizing PCA (principal component analysis), described and stated confidently the detection and analysis of a type of human ERA signal; however, based on qualitative analysis the authors proposed future work to validate their results with simultaneous measurement involving serosal or mucosal electrode recordings. In our study, the extracted signals satisfy the properties of the ERA signals reported in the literature in which invasive recordings were made in animals. It is important to notice that through the DCA process the ECA and ERA components can be extracted in time domain regardless of the other components because we extract only the desired component with a given characteristic.

Furthermore, the progressive increase in amplitude of the signal through three epochs can be easily seen (figure 7), demonstrating the ERA component during the post-prandial epoch. The energy increase can be seen in all volunteers, as shown in figure 13 and table 1. A wide variation of this index can noticed in the pre- and post-prandial epoch and among different subjects. This is due to several factors: differences in stomach muscle tonus and the shape of the body and fat layer can change the proximity of the stomach to the detector. It is valid to compare the epochs from one subject, but inter-subject comparison can only be made in relative terms. This method and results have not been reported previously.

Recordings using invasive methods (Akin and Sun 1999) show that the ERA component is time locked with the ECA component. In this work, using MGG, a non-invasive method, along with DCA and time–frequency analysis, we found that the ERA component was time locked with the ECA component, which agrees with the previous invasive methods.

We conclude that from MGG recordings DCA can be used very successfully to detect the electric response activity in normal volunteers. Further improvements in signal processing and standardization of signal acquisition are necessary to ascertain its possible use in clinical situations to identify and study gastric diseases.

Acknowledgments

This work was partially supported by the Brazilian agencies CNPq, FAPESP and CAPES.

References

Akin A and Sun H H 1999 Time–frequency methods for detecting spike activity of stomach *Med. Biol. Eng. Comput.* **37** 381–90

Andrä W and Nowak H 2006 *Magnetism in Medicine: A Handbook* (New York: Wiley-VCH)

Barros A K and Cichocki A 2001 Extraction of specific signals with temporal structure *Neural Comput.* **13** 1995–2003

Bradshaw L A, Irimia A, Sims J A, Gallucci M R, Palmer R L and Richards W O 2006 Biomagnetic characterization of spatiotemporal parameters of the gastric slow wave *Neurogastroenterol. Motility* **18** 619–31

Chen J D and McCallum R W 1993 Clinical-applications of electrogastrography *Am. J. Gastroenterol.* **88** 1324–36

de Araujo D B, Barros A K, Estombelo-Montesco C, Zhao H, da Silva A C R, Baffa O, Wakai R and Ohnishi N 2005 Fetal source extraction from magnetocardiographic recordings by dependent component analysis *Phys. Med. Biol.* **50** 4457–64

Irimia A, Richards W O and Bradshaw L A 2006 Magnetogastrographic detection of gastric electrical response activity in humans *Phys. Med. Biol.* **51** 1347–60

Jensen O, Gelfand J, Kounios J and Lisman J E 2002 Oscillations in the alpha band (9–12 Hz) increase with memory load during retention in a short-term memory task *Cereb. Cortex* **12** 877–82

Kato H, Naniwa S and Ishiguro M 1996 A bayesian multivariate nonstationary time series model for estimating mutual relationships among variables *J. Econometrics* **75** 147–61

Liang H, Lin Z and McCallum R W 2000 Artifact reduction in electrogastrogram based on empirical mode decomposition method *Med. Biol. Eng. Comput.* **38** 35–41

Liu L W C, Sperelakis N and Huizinga J D 1995 *Pacemaker Activity and Intercellular Communication in the Gastrointestinal Musculature* (Boca Raton, FL: CRC Press)

Madisetti V K and Williams D B (ed) 1997 *The Digital Signal Processing Handbook* (Boca Raton, FL: CRC Press)

Moraes E R and Baffa O 1999 Modelling of the magnetogastrogram *11th Int. Conf. Biomagnetism* ed T Yoshimoto *et al* (Sendai: Tohoku University Press) pp 262–5

Moraes E R, Troncon L E A, Baffa O, Oba-Kunyioshi A S, Wakai R and Leuthold A 2003 Adaptive, autoregressive spectral estimation for analysis of electrical signals of gastric origin *Physiol. Meas.* **24** 91–106

Smout A J P M, Vanderschee E J and Grashuis J L 1980 What is measured in electrogastrography *Dig. Dis. Sci.* **25** 179–87

TallonBaudry C, Bertrand O, Delpuech C and Pernier J 1997 Oscillatory gamma-band (30–70 Hz) activity induced by a visual search task in humans *J. Neurosci.* **17** 722–34

Toni A 2002 *Nonparametric statistical analysis of time–frequency representations of magnetoencephalographic data* Department of Electrical and Communications Engineering, S-114, Cognitive Technology